Integrated Continuous-to-Continuous Forward Modelling and Rebinning Strategies for Low-Dose CT with Flying Focal Spot

Piotr Pluta[1][0000−0003−4185−1971], Anna Jezuita[2][0000−0002−6188−0545], and Robet Cierniak[1][0000−0003−3465−7580]

[1] Department of Artificial Intelligence, Czestochowa University of Technology, Armii Krajowej 36, 42-200 Czestochowa, Poland
piotr.pluta@pcz.pl
[2] Faculty of Science and Technology, Jan Dlugosz University, Al. Armii Krajowej 13/15, 42-200 Czestochowa, Poland

Abstract. The study presents a reconstruction approach tailored to the demands of low-dose, single-slice computed tomography, emphasizing both radiation reduction and high computational efficiency. By focusing on scenarios in which only one diagnostically relevant slice is needed, the method avoids the overhead of volumetric processing and delivers images in a fraction of the time required by conventional algorithms. Although the highest spatial frequencies appear slightly softened, the reconstructed slices maintain sufficient diagnostic quality for rapid clinical assessment. This trade-off is particularly advantageous in emergency settings, where immediate visualization is more important than maximal sharpness. The approach therefore offers a practical solution for trauma care, accident evaluation, and other time-critical situations in which fast, low-dose imaging supports urgent medical decisions. Future extensions may incorporate artificial intelligence to enhance fine-detail recovery and adapt reconstruction quality to varying dose levels, creating a hybrid framework that combines the reliability of physics-based modeling with the flexibility of data-driven enhancement.

Keywords: low-dose computed tomography · emergency imaging · fast image reconstruction · flying focal spot · rebinning · continuous forward model · statistical iterative reconstruction

1 Introduction and motivation

Low-dose or ultra-low-dose CT requires reconstruction methods that preserve diagnostic image quality while minimizing radiation exposure, which shapes both the motivation and technical priorities of current research [5]. Reducing dose decreases photon counts, increases noise, and makes the reconstruction problem more ill-posed. In this context, the reconstruction algorithm becomes as important as the acquisition protocol itself: it must extract maximal information from limited, noisy measurements while avoiding artifacts. This motivates the development of models that more faithfully represent CT physics and remain effective when data are sparse or degraded.

ICCS Camera Ready Version 2026
To cite this paper please use the final published version:
DOI: 10.1007/978-3-032-29912-3_37

A second key motivation is reconstruction speed. Many iterative or model-based approaches achieve high image quality but are computationally expensive, especially for full 3D volumes. In many clinical scenarios, however, only a single diagnostically relevant slice is required. As recent studies show, traditional x-ray imaging is often insufficient for reliable diagnosis in acute settings [9]. In such cases, volumetric CT processing becomes unnecessary overhead. Methods optimized for fast, single-slice reconstruction can therefore reduce latency, lower hardware requirements, and support real-time clinical workflows.

Taken together, these considerations highlight the need for a reconstruction framework that is physically accurate, computationally lightweight, and suited to situations where rapid access to a single slice is more valuable than full volumetric precision. The following section introduces our proposed approach, which forms the theoretical foundation of our work.

2 Rebinning algorithm for FFS geometries

To address these requirements, we adopt a geometric formulation that enables consistent and efficient manipulation of synthetic x-rays [7]. In this formulation, each synthetic x-ray is described by three fundamental components: the focal point, the shifted isocenter, and the detector position [6]. Representing all three as three-dimensional coordinates provides a unified geometric framework for defining and manipulating equiangular x-rays. Within this 3D representation, all subsequent computations-including ray comparison, detector selection, and projection interpolation are performed consistently. The general form of a synthetic x-ray is given by:

$$xray(F_x^T, F_y^T, F_z^T, Q_x, Q_y, Q_z, D_x, D_y, D_z, p, s_m, \alpha_\psi), \tag{1}$$

where T denotes the index of the focal spot. Thus, if two focal spots are used and shifted radially, the expression becomes:

$$xray(F_x^A, F_y^A, F_z^A, F_x^B, F_y^B, F_z^B, Q_x, Q_y, Q_z, D_x, D_y, D_z, p, s_m, \alpha_\psi), \tag{2}$$

where F denotes the synthetic focal points, Q the shifted isocenter, and D the synthetic detector coordinates. The parameter p represents the projection value, while s_m and α_ψ describe the corresponding parallel-beam parameters.

Figure 1 illustrates the geometric relationships between these parameters. After computing the synthetic x-ray, the algorithm identifies the most appropriate real x-rays from the measured data using a comparison procedure that evaluates the angular proximity between synthetic and real focal points. The real focal spot coordinates are computed as:

$$f_x = -(R^F + \delta R^T) \cdot \sin(\alpha + \delta\alpha^T), \tag{3}$$

$$f_y = (R^F + \delta R^T) \cdot \cos(\alpha + \delta\alpha^T), \tag{4}$$

$$f_z = \dot{z}_0 + \delta\dot{z}^T, \tag{5}$$

ICCS Camera Ready Version 2026
To cite this paper please use the final published version:
DOI: 10.1007/978-3-032-29912-3_37

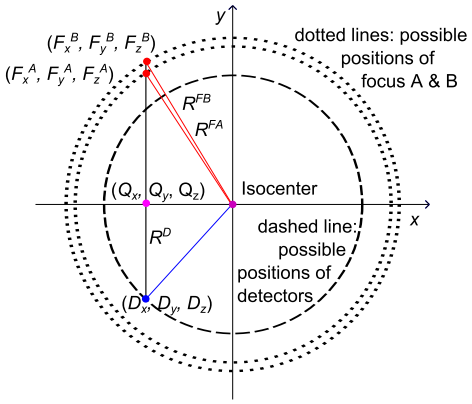

Fig. 1: Illustration of the X-ray parameter determination.

where T denotes one of the two focal spots and R^F is the nominal focal spot isocenter distance.

To determine which real x-rays best correspond to the synthetic one, the angle ζ between the real and synthetic focal points (relative to the shifted isocenter) is computed:

$$\zeta = \arccos\left(\frac{\hat{w}_x\hat{v}_x + \hat{w}_y\hat{v}_y}{\sqrt{\hat{w}_x^2 + \hat{w}_y^2}\cdot\sqrt{\hat{v}_x^2 + \hat{v}_y^2}}\right), \tag{6}$$

with

$$\begin{aligned} \hat{v}_x &= f_x^T - Q_x, \quad \hat{v}_y = f_y^T - Q_y, \\ \hat{w}_x &= F_x^T - Q_x, \quad \hat{w}_y = F_y^T - Q_y. \end{aligned} \tag{7}$$

Here, (f_x^T, f_y^T) correspond to the real focal spot coordinates, while (F_x^T, F_y^T) denote the synthetic ones.

After selecting the two nearest focal spots, the corresponding detector positions must be determined. This step is non-trivial because standard square-distance functions fail for rays parallel to the y-axis. Instead, a collinearity condition is applied. The real detector coordinates (D_x, D_y) satisfy:

$$\begin{cases} (D_x - f_{x_0})^2 + (D_y - f_{y_0})^2 = (R_D^T)^2, \\ (Q_x - f_x)(D_y - f_y) - (Q_y - f_y)(D_x - f_x) = 0, \end{cases} \tag{8}$$

ensuring that the detector lies on the correct circular arc and remains collinear with the focal spot and shifted isocenter.

Once the detector position is identified, the projection value for the synthetic detector is computed using trilinear interpolation, and the resulting value is assigned to the synthetic x-ray. These synthetic parallel-beam measurements are then used in the back-projection step of the iterative reconstruction algorithm (described in the next subsection). They may also serve as input for filtered back-projection, providing an initial estimate for iterative refinement.

ICCS Camera Ready Version 2026
To cite this paper please use the final published version:
DOI: 10.1007/978-3-032-29912-3_37

3 Statistical iterative reconstruction procedure

With the rebinning procedure established, we now integrate the resulting synthetic parallel-beam measurements into a statistical iterative reconstruction framework. The method follows the maximum-likelihood (ML) estimation paradigm [1, 8], well suited to low-dose CT due to its ability to model noise and compensate for sparse measurements. While conventional MBIR typically uses a discrete-to-discrete (D-D) formulation, our approach adopts an optimization strategy consistent with the continuous-to-continuous (C-C) data model [2]. A discretized version of this procedure is presented below. The optimization problem is defined as:

$$\mu_{\min} = \arg\min_{\mu} \left(\sum_{i=1}^{I} \sum_{j=1}^{J} \left(\sum_{\bar{i}} \sum_{\bar{j}} \mu^*(x_{\bar{i}}, y_{\bar{j}}) \cdot h_{\Delta i, \Delta j} - \tilde{\mu}(x_i, y_j) \right)^2 \right), \tag{9}$$

where the convolution kernel $h_{\Delta i, \Delta j}$ is given by:

$$h_{\Delta i, \Delta j} = \Delta_\alpha \sum_{\psi=0}^{\Psi-1} int(\Delta i \cos(\psi \Delta_\alpha) + \Delta j \sin(\psi \Delta_\alpha)), \tag{10}$$

with $int(\Delta s)$ denoting a linear interpolation function. The intermediate image $\tilde{\mu}(x_i, y_j)$ is obtained via back-projection of the synthetic parallel-beam measurements:

$$\tilde{\mu}(x_i, y_j) = \Delta_\alpha \sum_{\theta} \dot{p}(s_{ij}, \alpha_\psi), \tag{11}$$

where $\dot{p}(s_{ij}, \alpha_\psi)$ denotes the rebinned projection values.

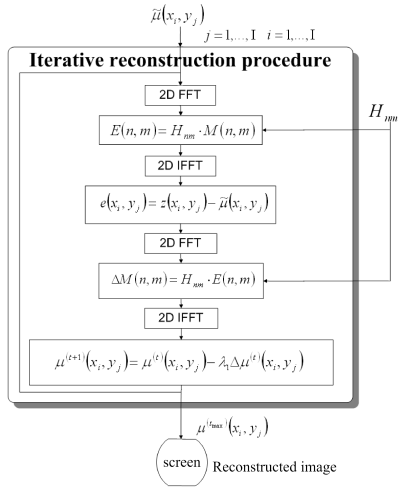

Fig. 2: Schematic representation of the iterative reconstruction procedure.

A key computational benefit of this approach is that the convolution kernel $h_{\Delta i, \Delta j}$ is iteration-independent and can therefore be precomputed, substantially

ICCS Camera Ready Version 2026
To cite this paper please use the final published version:
DOI: 10.1007/978-3-032-29912-3_37

accelerating the reconstruction process. Owing to the shift-invariant forward model, convolution is efficiently performed in the frequency domain, reducing computational complexity from N^4 to $8\log_2(4N^2)$. The FFT-based implementation supports image dimensions from 256×256 to 1024×1024. Although increasing resolution raises memory demands and computation time-scaling by a factor of four when the matrix size is doubled-the efficiency of the FFT formulation keeps reconstruction times within clinically acceptable limits.

4 Experiments and results (simulations, phantoms)

Having established the statistical iterative reconstruction framework and demonstrated its computational feasibility, we now evaluate its performance under controlled simulation conditions as well as with real clinical data. The goal of this section is to assess how effectively the proposed method handles varying noise levels, reduced-dose acquisition scenarios, and clinically relevant anatomical structures. To this end, we conducted a series of experiments using both mathematical phantoms and physical CT measurements.

In the initial phase of our computational experiments, we employed mathematical simulation data incorporating varying levels of noise. This artificially generated dataset allowed precise control over noise intensity in the acquired measurements. By systematically adjusting these conditions, we were able to explore the potential for reducing the x-ray radiation dose absorbed by a synthetic mathematical patient.

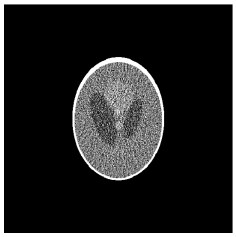

Fig. 3: ASSR reconstruction; Noise large.

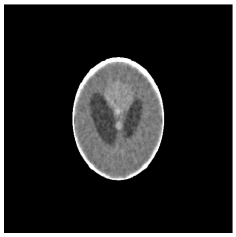

Fig. 4: ASSR + 5000 iteration; Noise large.

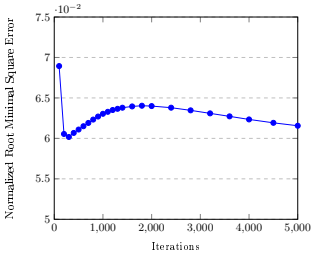

Fig. 5: NRMSE plot for ASSR + Iter; Noise large.

In the second phase, we utilized physical tomographic data obtained through our participation in the Low-Dose Grand Challenge. In this scenario, full-dose physical data were modified to simulate quarter-dose x-ray exposure. While this approximation provides valuable insights, it naturally introduces limitations in accurately assessing the true extent of dose reduction.

Our primary computational simulations were based on the well-known Shepp-Logan mathematical phantom. When simulating projection systems using a conical beam rotating around the patient, a three-dimensional phantom must be defined. The 3D version of the Shepp-Logan model consists of multiple ellipsoids [4], which represent simple yet effective geometric structures for constructing

ICCS Camera Ready Version 2026
To cite this paper please use the final published version:
DOI: 10.1007/978-3-032-29912-3_37

mathematical phantoms. This ellipsoid-based phantom facilitates the computation of projection values for all rays at arbitrary projection angles.

Figures 3 and 4 show phantom reconstructions at $z = 0$, while Figure 5 reports the iteration-wise evolution of NRMSE. Conventional FBP with ASSR (Fig. 3) is compared with the proposed iterative ASSR method under high-noise conditions (Fig. 4). The iterative approach substantially reduces reconstruction error, lowering MSE from 917.1249 to 241.0189, accompanied by improvements in NRMSE (0.11875 to 0.06084) and SSIM (0.87735 to 0.96750).

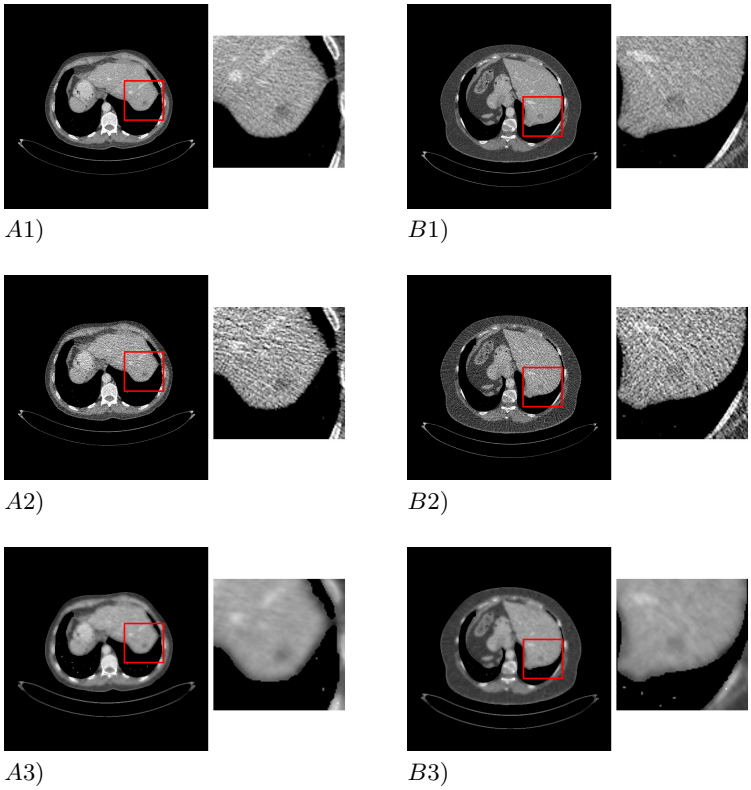

Fig. 6: Views of the images, patient A and B: reconstructed image using the ASSR method with full dose (at the top - A1, B1), and using $\frac{1}{4}$ dose (in the middle - A2, B2); reconstructed image using the statistical approach presented in this paper (at the bottom - A3, B3).

To further evaluate this applicability, we conducted experiments using data from a commercial CT scanner. Reconstructions were performed with both full-dose measurements (standard x-ray intensity for liver examinations) and simulated quarter-dose data. The scans were acquired using a Siemens AG Somatom medical scanner (Forchheim, Germany) in helical mode with a tube potential of 120 kVp and a tube current of 200 mAs. Figures 6A and 6B present reconstructed images of two patients at simulated quarter dose. Each figure compares

ICCS Camera Ready Version 2026
To cite this paper please use the final published version:
DOI: 10.1007/978-3-032-29912-3_37

full-dose reconstructions using the ASSR method, quarter-dose reconstructions using ASSR, and quarter-dose reconstructions using our ASSR with statistical iterative approach.

For our method, all reconstructions were generated after 5000 iterations, which proved sufficient to resolve clinically relevant details. Although radiologists initially recommended 7000 iterations [3], optimization demonstrated that equivalent image quality could be achieved with fewer iterations. The reconstructed images contain various lesion types (previously diagnosed by radiologists), with affected regions marked by red rectangle.

Quantitative comparisons between full- and quarter-dose reconstructions are summarized in Table 1. Across all patients, our statistical iterative method consistently achieved lower MSE and NRMSE values than the ASSR method, confirming its superior performance under reduced-dose conditions.

Table 1: MSE, NRMSE and SIMM results for reconstructed patient cross-sections, comparing full-dose and quarter-dose scans for ASSR and ASSR with statistical iterative method.

Patient	Measured method		
No.	MSE	NRMSE	SSIM
1 (Figure 6 A2) - ASSR	197,54300	0,05511759	0,9680605
2 (Figure 6 B2) - ASSR	349,69790	0,07333399	0,9399601
1 (Figure 6 A3) - ASSR+Iter	17,58809	0,01644598	0,9968895
2 (Figure 6 B3) - ASSR+Iter	19,41735	0,01728036	0,9961087

5 Conclusion

The study demonstrates that fast, low-dose, single-slice CT reconstruction can effectively meet the needs of clinical situations where rapid decision-making is essential and full volumetric imaging is unnecessary. By prioritizing minimal radiation exposure and extreme computational efficiency, the method delivers diagnostically useful images within a fraction of the time required by conventional approaches. Although the highest spatial frequencies appear slightly softened, this trade-off is justified in emergency contexts where immediate visualization outweighs the need for maximal sharpness. The approach therefore offers a practical pathway toward safer and faster CT imaging, particularly suited for trauma care, accident victims, and other time-critical scenarios in which rapid access to a single, reliable slice can guide urgent clinical intervention. Future work will explore integrating modern AI methods to improve both image quality and reconstruction speed. Deep learning models trained on low-dose CT data may help restore high-frequency details while maintaining real-time performance, as suggested by recent frequency-aware denoising studies [10, 11]. Incorporating AI-based denoisers, learned priors, or hybrid physics-informed networks into the pipeline could yield a next-generation framework that merges the robustness of physics-based modelling with the flexibility of machine learning.

Acknowledgments. The authors thank Dr. Cynthia McCollough and the American Association of Physicists in Medicine for providing the Low-Dose CT Grand Challenge dataset.

ICCS Camera Ready Version 2026
To cite this paper please use the final published version:
DOI: 10.1007/978-3-032-29912-3_37

Institutional review. Ethical review and approval were waived for this study because all data had been made available upon participation in the Low-Dose CT Grand Challenge by Dr. Cynthia McCollough and the American Association of Physicists in Medicine.

Funding. This research received no external funding.

Disclosure of Interests. The authors declare no conflicts of interest.

References

1. Bouman, C., Sauer, K.: A unified approach to statistical tomography using coordinate descent optimization. IEEE Transactions on Image Processing **5**(3), 480–492 (1996). https://doi.org/10.1109/83.491321
2. Cierniak, R., Pluta, P.: Statistical iterative reconstruction algorithm based on a continuous-to-continuous model formulated for spiral cone-beam CT. Journal of Artificial Intelligence and Soft Computing Research pp. 613–620 (2020). https://doi.org/10.1007/978-3-030-50420-5_46
3. Cierniak, R., Pluta, P., Waligóra, M., Szymański, Z., Grzanek, K., Pałka, F., Piuri, V.: A new statistical reconstruction method for the computed tomography using an x-ray tube with flying focal spot. Journal of Artificial Intelligence and Soft Computing Research **11**(4), 271–286 (2021). https://doi.org/https://doi.org/10.2478/jaiscr-2021-0016
4. Kak AC, S.M.: Principles of Computerized Tomographic Imaging. IEEE Press, New York (1988)
5. Pan, Z., Zhang, Y., Zhang, L., Wang, L., Zhao, K., Li, Q., Wang, A., Hu, Y., Xie, X.: Detection, measurement, and diagnosis of lung nodules by ultra-low-dose ct in lung cancer screening: a systematic review. BJR|Open **6**(1) (Dec 2023). https://doi.org/https://doi.org/10.1093/bjro/tzae041
6. Pluta, P.: A New Approach to Statistical Iterative Reconstruction Algorithm for a CT Scanner with Flying Focal Spot Using a Rebinning Method, pp. 286–299. Springer International Publishing (2023). https://doi.org/10.1007/978-3-031-23480-4_24
7. Pluta, P., Nieszporek, K., Sosnowski, J.: Positioning the reconstruction plane for a statistical iterative reconstruction algorithm with rebinning in ct scanners with a flying focal spot pp. 345–355 (2025). https://doi.org/10.1007/978-3-031-81596-6_30
8. Sauer, K., Bouman, C.: A local update strategy for iterative reconstruction from projections. IEEE Transactions on Signal Processing **41**(2), 534–548 (1993). https://doi.org/10.1109/78.193196
9. Tækker, M., Graumann, O.: Ultra-low-dose ct—a new imaging modality in the diagnostic workflow of an emergency department? European Radiology **35**(8), 4834–4835 (Apr 2025). https://doi.org/https://doi.org/10.1007/s00330-025-11569-2
10. Yang, C., Zhang, C., Shen, H., Peng, T., Wang, C., Deng, L., Chen, H., He, L.: Hfan: High-frequency attention network for hyperspectral image denoising. International Journal of Machine Learning and Cybernetics **15**(3), 837–851 (Aug 2023). https://doi.org/https://doi.org/10.1007/s13042-023-01942-2
11. Zhang, K., Zuo, W., Zhang, L.: Ffdnet: Toward a fast and flexible solution for cnn-based image denoising. IEEE Transactions on Image Processing **27**(9), 4608–4622 (Sep 2018). https://doi.org/10.1109/TIP.2018.2839891

ICCS Camera Ready Version 2026
To cite this paper please use the final published version:
DOI: 10.1007/978-3-032-29912-3_37